Journal of Cerebral Blood Flow & Metabolism (2011) 31, 693–705

www.jcbfm.com

Astrocytes and pericytes differentially modulate blood–brain barrier characteristics during development and hypoxic insult

Abraham Al Ahmad[1,2], Carole Bürgi Taboada[1], Max Gassmann[1] and Omolara O Ogunshola[1]

[1]*Institute of Veterinary Physiology, Vetsuisse Faculty and Zurich Centre for Integrative Human Physiology (ZIHP), University of Zürich, Switzerland;* [2]*Department of Molecular and Cellular Medicine, Texas A&M Health Science Center, College Station, Texas, USA*

Understanding regulation of blood–brain barrier (BBB) is crucial to reduce/prevent its disruption during injury. As high brain complexity makes interpretation of *in vivo* data challenging, BBB studies are frequently performed using simplified *in vitro* models. However, many models fail to address the three-dimensional (3D) cellular interactions that occur *in vivo*, an important feature that may explain discrepancies in translation of *in vitro* data to the *in vivo* situation. We have designed and characterized an innovative 3D model that reproduces morphological and functional characteristics of the BBB *in vivo* and used it to investigate cellular interactions and contribution of astrocytes and pericytes to BBB development. Our model shows that both astrocytes and pericytes significantly suppress endothelial proliferation. In contrast, differential effects on tubulogenesis were observed with astrocytes reducing the number of tubes formed but increasing diameters and length, whereas pericytes had the opposite effect. Pericytes also induce proper localization of barrier proteins, lumen polarization, and functional activity of ATP-binding cassette (ABC) transporters similar to astrocytes, but the presence of both cells is required to maintain optimal barrier characteristics during hypoxic exposure. This model is simple, dynamic, and convenient to study many aspects of BBB function and represents an exciting new tool to address open questions of BBB regulation.
Journal of Cerebral Blood Flow & Metabolism (2011) **31,** 693–705; doi:10.1038/jcbfm.2010.148; published online 8 September 2010

Keywords: blood–brain barrier; *in vitro* model; microscopy; neurovascular unit; vascular biology

Introduction

The blood–brain barrier (BBB) constitutes a neurovascular unit formed by microvascular endothelial cells (ECs), pericytes, and perivascular astrocytes (Hawkins and Davis, 2005). The ECs of the BBB display a specialized phenotype characterized by the presence of tight junctions (TJs) that limit diffusion of water-soluble compounds from the blood to the brain tissue (Brightman and Reese, 1969). In addition, the barrier acts as a selective filter toward lipophilic molecules by expression of ATP-binding cassette (ABC) transporters in their luminal and abluminal compartments (Soontornmalai *et al*, 2006; Warren *et al*, 2009). Astrocytes have been well documented to induce barrier properties in brain ECs both *in vitro* (Al Ahmad *et al*, 2009; Dehouck *et al*, 1990) and *in vivo* (Janzer and Raff, 1987; Zerlin and Goldman, 1997); however, the nature of the factors involved and, in particular, the role of pericytes is only now becoming more evident (Al Ahmad *et al*, 2009; Virgintino *et al*, 2007).

Disruption or dysfunction of the BBB constitutes a well-described hallmark of many neurologic diseases including Alzheimer's disease (Zlokovic, 2008), neuroAIDS (Banks *et al*, 2006), neuroinflammation (Engelhardt, 2008), Parkinson's disease (Zlokovic, 2008), and stroke (del Zoppo and Mabuchi, 2003; Kaur and Ling, 2008; Kulik *et al*, 2008; Lee *et al*, 2004). Elucidation of the cellular and molecular mechanisms by which vascular leakage is induced during disease is dramatically limited due to the major technical challenges faced when using *in vivo* models. Simplified *in vitro* models represent an important and frequently used alternative for investigation of BBB function and alterations. However, despite constantly increasing knowledge of the cellular and molecular mechanisms underlying BBB

Correspondence: Dr OO Ogunshola, Institute of Veterinary Physiology, Vetsuisse Faculty of the University of Zurich, Winterthurerstrasse 260, 8057 Zürich, Switzerland.
E-mail: larao@access.uzh.ch; http://www.vetphys.unizh.ch
This study was supported by Swiss Stiftung 3R (contract grant sponsor, grant number 93/04).
Received 18 December 2009; revised 20 July 2010; accepted 21 July 2010; published online 8 September 2010

physiology and pathophysiology, the ability to translate *in vitro* findings to *in vivo* situation remains suboptimal (Neuwelt *et al*, 2008). Obviously, many discrepancies between these *in vitro* systems and the *in vivo* situation are a major cause of this shortfall. In particular, the absence of appropriate three-dimensional (3D) cellular structure, organization, and specific cell–cell interactions may represent important features omitted in the current models. Thus, the development of new *in vitro* systems that are more representative of native BBB structure and allow dynamic movement and reorganization of cells in response to a changing environment are sorely needed.

In this study, we have developed an innovative 3D BBB model based on collagen extracellular matrix (Koh *et al*, 2008; Ment *et al*, 1997). This model remarkably allows each cell of the BBB to display their unique morphology as occurs *in vivo*. Within this matrix, brain ECs formed patent vascular structures that are contacted by astrocytes and pericytes. Our study shows that interactions between ECs and astrocytes and pericytes distinctly modulate EC proliferation, tube morphogenesis, induction of barrier properties, and vascular polarity. We further use this innovative research tool to investigate dynamic changes in cellular interactions, and the specific contribution of each cell type to vascular alterations, during the pathological condition of oxygen deprivation. This versatile model will undoubtedly improve our understanding of the cellular and molecular mechanisms underlying BBB regulation during physiological and pathological situations.

Materials and methods

All experiments were performed in accordance with Swiss animal protection laws and University of Zürich institutional guidelines for animal experimentation.

Cell Culture

Rat brain endothelial cell line (RBE4; Roux *et al*, 1994) from passages 45 to 55 were cultured on gelatin-coated dishes (Corning Inc, Corning, NY, USA) as previously described (Al Ahmad *et al*, 2009). Primary rat astrocytes were isolated from neonatal pups as described previously (Chow *et al*, 2001). Primary rat brain pericytes were obtained from adult rat brains and isolated following the protocol established by Dore-Duffy (2003). Freshly isolated pericytes were cultured in Dulbecco's modified Eagle medium (DMEM) supplemented with 20% fetal bovine serum, 50 mg/mL gentamycin sulfate and 2.5 mg/mL amphotericin B until near confluency. Purity of all primary cultures was confirmed using cell-specific markers as previously described (Al Ahmad *et al*, 2009).

Collagen Matrix

Rat-tail collagen was extracted following a method established by Bell *et al* (1979). Briefly, rat-tail tendrils were sectioned, minced, and dissolved overnight at 4°C in 15 mmol/L acetic acid solution (Sigma-Aldrich, Buchs, Switzerland). Debris was removed by ultracentrifugation for 1 hour at 20,000 *g* at 4°C (RC 5C Plus, Sorvall Products, Newton, CT, USA). Soluble collagen I was lyophilized using a vacuum desiccator (RC 10.10, Jouan, Saint Herblain, France) and stored at −20°C. Working collagen I solution (2.5 mg/mL) was prepared in 15 mmol/L acetic acid.

Three-Dimensional Cell Culture

The procedure for 3D cell culture is schematized in Figure 1A. In brief, collagen solution was mixed with 1/10th volume of 10× Earle's balanced salt solution (Sigma-Aldrich) containing phenol red then neutralized with 1 N NaOH solution (Sigma-Aldrich). The ECs were added at a density of 5×10^5 cells/mL in monoculture experiments. For coculture experiments, RBE4 cells, astrocytes, and pericytes were cultured in ratios that are estimated to occur *in vivo*, namely 1:5:1, in accordance with the literature (Pardridge, 1999). The collagen single-cell suspension was disposed as droplets onto 60 mm Petri dishes (Nunc, Roskilde, Denmark) then incubated at 37°C to allow gel solidification. Collagen droplets were overlaid with RBE4 medium and incubated at 37°C with 5% CO_2. Medium was replaced after 3 days of culture.

Cell Density Determination

To facilitate cell counting, collagen matrix was dissociated by incubation for 20 minutes at 37°C in collagen digestion buffer (1 mg/mL collagenase, 0.1 mmol/L $CaCl_2$, 1 mmol/L $MgCl_2$). Cells were centrifuged for 5 minutes at 1000 *g* then resuspended in 100 μL of medium. Cell suspension was mixed 1:1 with 0.4% Trypan Blue (Sigma-Aldrich) prepared in phosphate-buffered saline (PBS) and cell density was determined using a glass hematocytometer (Neubauer, Brand, Wertheim, Germany). For both monocultures and cocultures, total cell density at each time point is expressed as fold increase compared with the control time point (i.e., immediately after seeding).

Morphological Analysis

To determine tube number, length, and diameter, whole mounted collagen droplets were observed using inverted fluorescence microscope (Axiovert 200M, Carl Zeiss, Feldbach, Switzerland) in brightfield mode. Micrograph pictures were acquired with a ×10 objective using an 8-bit CCD camera (Axiocam HRm, Carl Zeiss) and processed using Axiovision 4.6 software (Carl Zeiss). The different features were determined using the measure tool included in Axiovision software package.

Enzyme-Linked Immunosorbent Assay Measurements

Quantitation of secreted levels vascular endothelial growth factor (VEGF), platelet derived growth factor (PDGF)-AB, and transforming growth factor (TGF)-β1 in culture media were performed using Quantikine ELISA kits (R&D Systems Europe, Abingdon, UK) according to the manufacturer's instructions. Optical densities were measured using a microplate reader (Multiskan RC; Thermo

Labsystems, Helsinki, Finland) at 450 nm, with wavelength correction at 570 nm.

Quantitative Real-Time PCR

Total RNA was isolated directly from collagen droplets using TRIzol reagent (Invitrogen, Carlsbad, CA, USA). A measure of 2 μg of total RNA per sample was then reverse transcribed using the ImProm-II ReverseTranscriptase (Promega, Madison, WI, USA) according to the manufacturer's instructions. Quantitative real-time PCR was performed with an ABI 7500 Fast Real-Time PCR System using the Power SybrGreenPCR Master Mix (Applied Biosystems, Foster City, CA, USA). The following primers were used: fgf2, 5′-AACGGCGGCTTCTTCCTGCG-3′ and 5′-TGG CCTTCTGTCCAGGCCCC-3′; flt1, 5′-GCCGAGGACGCAGG GGACTA-3′ and 5′-GACAGGGGTGCCACAGCCAC-3′; gapdh, 5′-GAGGACCAGGTTGTCTCCTG-3′ and 5′-ATGTAGGCCATG AGGTCCAC-3′; vegfr2, 5′-ACACACAGCGAGCACCGAGC-3′ and 5′-GAGCGGAAGCGTGCCCCTTT-3′; tie2 5′-AAGGCCTCT GGCTGGCCACT-3′ and 5′-TTTGGGGCATGCAGGGGCTC-3′. All data were normalized to gapdh, and fold changes were calculated by the comparative *Ct* method ($\Delta\Delta Ct$ method).

Immunocytochemistry

After 6 days of culture, droplets were washed with cold PBS and fixed with 4% paraformaldehyde solution then permeabilized with 0.1% Triton X-100 solution and blocked with 10% normal goat serum for 4 hours at room temperature. Droplets were incubated overnight at 4°C with primary antibodies raised against CD31 (1:100, Chemicon, Millipore, Zug, Switzerland); glial fibrillary acidic protein (1:100, Sigma-Aldrich), α-smooth muscle actin isoform (1:100, Sigma-Aldrich), zonula occludens-1 (ZO-1; 1:100, Invitrogen), claudin-5 (1:100, Invitrogen), β-catenin (1:100, Chemicon), Tie2 (1:100, Santa Cruz Biotechnology, Heidelberg, Germany), P-glycoprotein (P-gp; 1:100, Calbiochem, VWR, Dietikon, Switzerland), utrophin and multidrug resistant protein-2 antibodies (a gift from Dr JM Fritschy). Detection was performed using either Alexa-488 or Alexa-546-conjugated antibodies (Invitrogen). Because of the absence of a well-accepted pericyte-specific marker, to simultaneously observe all three cell types pericytes were prelabeled with DiD a far-red fluorescent lipophilic dye (Invitrogen) following the manufacturer's instructions. Samples were observed using a Leica confocal microscope (Leica SP2, Leica Microsystems, Heerbrugg, Switzerland) and acquired with Leica Confocal Software. To obtain 3D image reconstructions, a stack of 70 to 80 micrograph pictures were acquired for each sample, maintaining a thickness of 0.5 μm between each focal plan, and processed by Imaris 6.0 software (Bitplane, Zurich, Switzerland). Image reconstruction also enabled creation of virtual *z*-stack cross-section images.

Transmitted Electron Microscopy

Droplets were fixed with 3% glutaraldehyde buffer, postfixed with 2% OsO_4 buffer, and dehydrated with 70% to 100% ethanol-containing solutions. Dehydrated samples were embedded into Epon 813 resin (Epon, Hexion, Rotterdam, The Netherlands), and 70 nm slices were cut using a diamond-knife ultramicrotome. Sections were observed using a transmission electron microscope (CM-100, Philips Research, Eindhoven, The Netherlands). Micrograph pictures were obtained using a 12-megapixel digital camera (Gatan GmbH, München, Germany) and Digital Micrograph software (Gatan GmbH). Images were processed using ImageJ 1.41 (ImageJ, NIH, Bethesda, MD, USA).

P-Glycoprotein Activity Assay

P-glycoprotein activity was assessed by live imaging confocal microscopy based on (*N*-(4-nitrobenzofurazan-7-yl)-D-Lys^8)-cyclosporin A (NBD-CsA) luminal accumulation assay with some modification of the original protocol established by Miller *et al* (2000). Briefly, fresh living 6-day-old cultures were incubated in PBS containing 2 mmol/L NBD-CsA (gift from Dr B Bauer) for 1 hour at 37°C then transferred to slide glass chambers (Lab-Tek II, Nunc) filled with warm PBS and observed with a confocal microscope using a $\times 20$ oil immersion objective (Leica SP2, Leica). Cross-sections were obtained by image reconstruction following the same methodology cited previously. Inhibition experiments were performed by addition of either 1 mM KCN (Sigma-Aldrich) or 10 μmol/L verapamil (Sigma-Aldrich) to incubation medium as well as the PBS solution used for the microscopy observations, according to the original protocol.

O_2 Deprivation Stress Experiments

Experiments were performed in a purpose-built hypoxic glove-box chamber (InVivO$_2$ 400, Ruskinn Technologies, Pencoed, UK) maintained at 37°C with 5% CO_2. Culture droplets were exposed to 1% O_2 for up to 48 hours.

Statistical Analysis

All results are expressed as mean ± s.d. of at least four or more independent experiments. Statistical significance was assessed using one-way and two-way analysis of variance. P values < 0.05 were considered significant.

Results

The Three-Dimensional Collagen Matrix Supports Endothelial Tubulogenesis and Appropriate Multicellular Cellular Interactions

The RBE4 cells exhibit vasculogenic and angiogenic-like features when cultured inside a 3D collagen matrix (Figure 1B). In the collagen matrix, RBE4 quickly formed multicellular cysts within 24 hours of culture (upper panels), rapidly followed by formation of intercystal connections by Day 2. After 4 days of culture, these intercystal connections changed morphology and were progressively replaced by

thicker tubular structures denominated as 'tube-like structures.' These tubes displayed longer and thicker processes than intercystal connections, but also presented branching processes (see Supplementary Figure S1). An examination of the different structures using different fluorescent cellular markers (Figure 1B) revealed that such features were multicellular complexes. In conclusion, 3D collagen-based matrices allow cell motility and also support tubulogenesis of these cells.

We next cocultured RBE4 cells with astrocytes and pericytes and examined cell morphology using cell-specific markers (Figures 1C–1F). The presence of either astrocytes (Figure 1C) or pericytes (Figure 1D) did not interrupt formation of endothelial tube-like structures. Indeed, astrocytes cocultured with RBE4

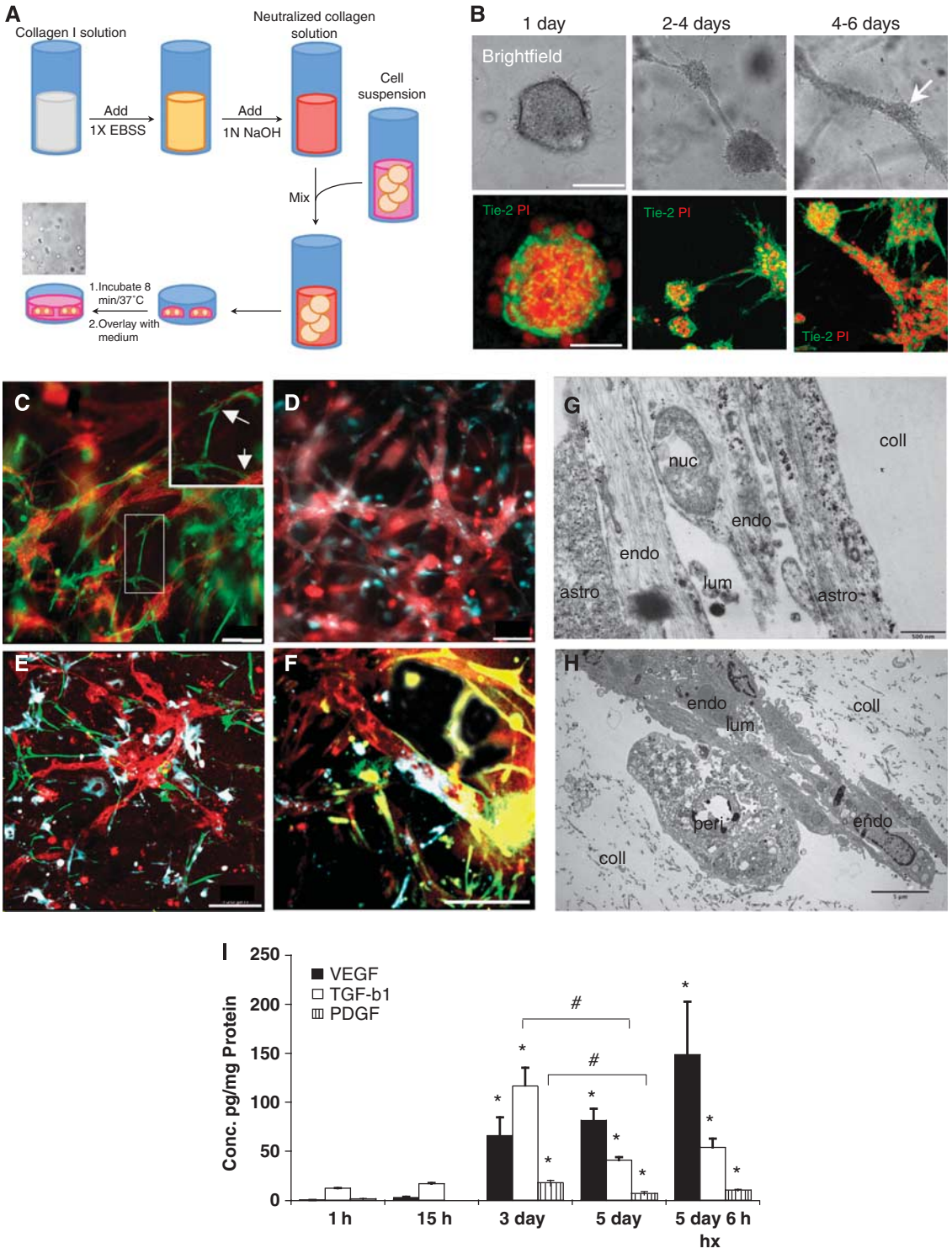

cells formed processes (green, and arrows in high power insert) that contacted the EC tubes (red), whereas pericytes rather appeared to overlap them with their whole cell bodies (blue). The presence of both astrocytes and pericytes (Figures 1E and F) did not interfere either with the endothelial tubulogenesis or the cellular interactions. Electron microscopy on these cocultures (Figures 1G–1H) revealed that astrocyte processes (Figure 1G) and pericytes (Figure 1H) physically contacted the RBE4 tubes. Notably, we observed the presence of a lumen within the tubes confirming the structures as analogous to *in vivo* capillaries.

Expression Profiles of Angiogenic Factors During Three-Dimensional Culture Development

To confirm that our model reproduces expression profiles associated with angiogenesis *in vivo*, secretion of some well-defined angiogenic molecules over time was measured. We used QPCR (see Supplementary Figure S2) and enzyme-linked immunosorbent assay to assay levels of classical angiogenic mediators secreted into the culture media. Our data clearly show that VEGF, PDGF, and TGF-β1 concentrations are significantly increased, resulting in their accumulation in the media after 3 days of culture (Figure 1I). This time point corresponds to the period of rapid tubulogenesis occurring in our model system. After 5 days of culture, VEGF levels remain stable, whereas PDGF and TGF-β1 concentrations decrease correlating well with reduced tubulogenesis and the more mature vascular phenotype at this time. Of note, hypoxic exposure for 6 hours causes a further induction of VEGF secretion in accordance with the responsiveness of this gene to oxygen deprivation.

Astrocytes and Pericytes Oppositely Regulate EC Angiogenesis

The RBE4 cells cultured alone proliferate very rapidly within the collagen matrix, resulting in an increase of up to eightfold over 6 days of culture. Whereas pericyte monocultures also proliferated within the matrix, albeit it not as rapidly as RBE4 cells, astrocytes did not (see Supplementary Figure S3). Surprisingly, coculture of either astrocytes or pericytes with RBE4 completely abolished EC proliferation during culture (Figure 2A), although the presence of both cells partially supported proliferation. To evaluate the impact of both cells on tube formation, we quantified alterations in the number, length, and diameter of tube-like structures during culture genesis (Figures 2B–2D). Astrocyte coculture significantly reduced the number of tubes formed by $>50\%$ compared with RBE4 monocultures, indicating that astrocytes prevent the angiogenic-like process (Figure 2B). In contrast, pericytes increased tube numbers by $\sim 40\%$, indicating a predominantly proangiogenic role. The three-cell cocultures also had a strong inhibitory effect, suggesting that overall astrocytes dictate the EC angiogenic rate. Although astrocyte coculture limited the number of tubes, tube length was significantly increased (Figure 2C) compared with monocultures (median values of 208.7 and 154.3 μm, respectively). Pericytes alone had no effect, but the presence of both cells produced the longest tubes (median value of 227.0 μm). Astrocyte coculturing also increased tube diameter compared with ECs alone (20.53 μm versus 16.55 μm respectively), in contrast to pericytes (11.88 μm; Figure 2D). The presence of both cells resulted in diameters reminiscent of RBE4 monocultures (15.40 μm), indicating inhibition of both astrocyte and pericyte effects. Thus, coculturing blunts the pericytic proangiogenic effect seemingly tipping the balance in favor of astrocytes.

Coculture Is Necessary to Induce a Proper Blood–Brain Barrier Phenotype

Formation of appropriate adherens and tight junction complexes (AJ and TJ) constitute two important features of a mature BBB. We investigated whether these junctional proteins localize to cell borders in both monocultures and cocultures (Figure 3), as such observations are classically associated with TJ formation (Al Ahmad *et al*, 2009; Nakagawa *et al*,

Figure 1 Collagen three-dimensional (3D) matrix supports tube formation, appropriate cellular interactions, and time-dependent expression of angiogenic molecules. (**A**) Diagrammatical scheme of the experimental protocol used for the collagen-based 3D cell culture. (**B**) Within the collagen matrix, RBE4 cells undergo morphogenesis first forming cyst-like structures, then connections between the cysts that finally result in a complex network of multicellular tube-like structures. The RBE4 cells were stained with the cell-specific marker Tie-2 (green), and cell nuclei were stained with propidium iodide (PI, red). Scale bar = 50 μm. (**C**, **D**) Astrocytes and pericytes interact with RBE4 tubes in a similar manner as the *in vivo* situation. Note the glial fibrillary acidic protein (GFAP)-positive processes formed by astrocytes (green) over the RBE4 tube-like structures (red). Insert shows magnified image with arrows to highlight this interaction. In contrast, pericytes (DiD stain in blue) overlap RBE4 tubes. Scale bar = 100 μm. Low (**E**) and high power images (**F**) show that the presence of both astrocytes and pericytes did not alter tube morphology or cellular interactions. Astrocyte processes (green) and pericyte overlap (blue) are easily visible at the vessel walls. Scale bar = 100 μm. (**G**, **H**) Electron micrograph pictures of tubes within the matrix (coll) show the close physical contacts between RBE4 tubes (endo), astrocytes (astro, **G**), and pericytes (**H**, peri) as well as the presence of a lumen (lum). (**I**) Expression profiles of select angiogenic molecules show that secreted levels of VEGF, TGF-β1, and PDGF are significantly induced after 3 days of culture. Hypoxia further induces VEGF secretion, whereas TGF-β1 and PDGF concentrations remain unaffected. $n = 3$; $^{*}P < 0.05$ compared with 1 hour time point, $^{\#}P < 0.05$ at 3 days compared with 5-day time point.

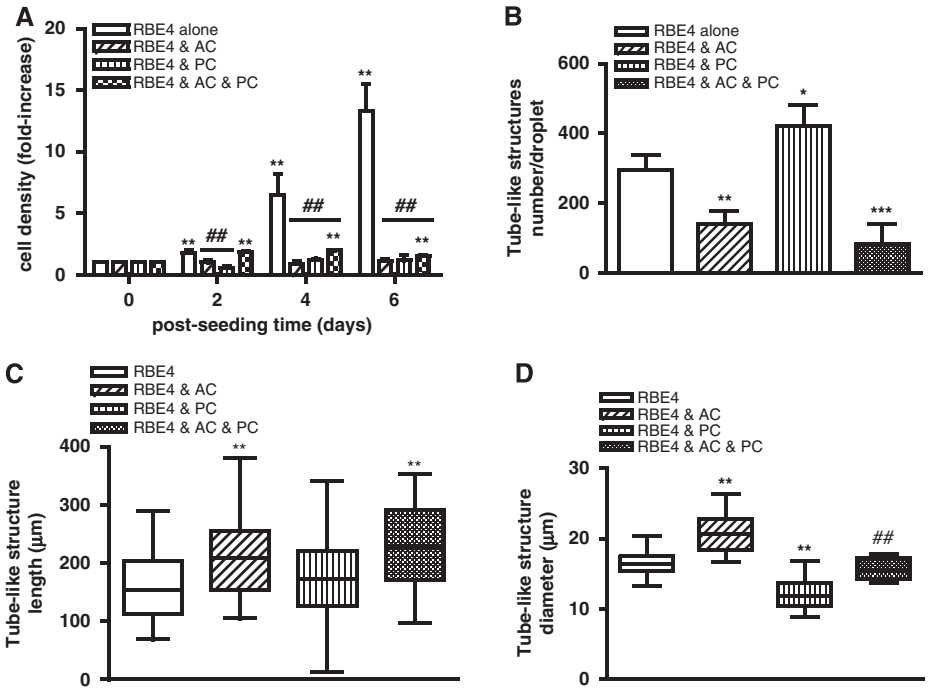

Figure 2 Astrocytes (AC) and pericytes (PC) differentially modulate RBE4 tube morphogenesis. (**A**) Cell density continuously increased in RBE4 monocultures. The AC or PC cocultures inhibited the increase in cell density compared with RBE4 monocultures, whereas the presence of both cells (black and white squares bars) supported a modest increase after 2 days of culture. $n = 4$; $^{**}P < 0.01$ compared with 0 day time point; $^{\#\#}P < 0.01$ compared with RBE4 monocultures. (**B**) AC and PC differentially modulate the number of RBE4 tubes formed after 6 days. Note the decreased number of tubes in the AC and three-cell cocultures compared with the PC group. $n = 4$; $^{*}P < 0.05$; $^{**}P < 0.01$ and $^{***}P < 0.001$ compared with RBE4 cells alone. (**C**) AC and three-cell cocultures induce longer tube-like structures. $n = 30$, $^{**}P < 0.01$ compared with RBE4 cell group. (**D**) The AC induces larger diameter tubes, and PC induces thinner diameter tubes. The presence of both AC and PC resulted in similar diameter size as RBE4 monocultures. $n = 30$; $^{**}P < 0.01$ compared with RBE4 monocultures, $^{\#\#}P < 0.01$ compared with two-cell cocultures.

2009). Analysis of tube-like structures from RBE4 monocultures showed β-catenin (Figure 3A) expression at cell borders, suggesting AJ complex formation. However, staining for the adhesion molecule CD31 (Figure 3E), as well as TJ proteins claudin-5 (Figure 3I) and ZO-1 (Figure 3M), appeared diffuse, indicating an inefficient BBB phenotype. In contrast, culture with astrocytes caused localization of all junctional proteins studied as well as CD31 to cell–cell borders (Figures 3B, 3F, 3J, and 3N) as expected, suggesting proper junctional complex formation and thus underlining the important role played by astrocytes during tube maturation. Although CD31 and ZO-1 localization in pericyte cocultures (Figures 3G and 3O, respectively) was similar to RBE4 monocultures, incidence of restricted claudin-5 staining at cell borders (Figure 3K) suggested partial TJ formation. As expected, the presence of both cells promoted formation of both AJ (Figures 3D and 3H) and TJ (Figures 3L and 3P) complexes, as observed by the strong positive staining delimiting the cell borders.

To further confirm these observations, we carried out additional analysis of 3D culture electron microscopy samples. Notably, in three-cell cocultures, we observed the presence of electron-dense particles at specific regions of endothelial cell–cell interactions, indicating the formation of TJs (Figure 3Q). In comparison, these junctional structures were absent in endothelial monocultures (Figure 3R). Taken together, our data suggest that interactions with astrocytes and pericytes are required to induce formation of BBB-specific TJ complexes in 3D cultures.

Endothelial cell Lumen Polarization Requires the Presence of Astrocytes and Pericytes

To further establish the contribution of astrocytes and pericytes to formation of a BBB phenotype, tube polarity was investigated. We performed double immunocytochemistry for multidrug resistance proteins and the EC-specific markers Tie-2 and CD31 (notably the distribution of CD31 and Tie-2 is not polarized) followed by confocal microscopy and *z*-stack image reconstruction (Figures 4A–4L).

We first investigated lumen polarization using utrophin, a cytoskeleton protein localized at the abluminal face in EC cells. Tube cross-sections from RBE4 monocultures (Figure 4A) and cocultures (Figures 4B–4D) revealed utrophin localization (green) at the abluminal face of tube structures (red), indicating that ECs alone as well as in cocultures properly localize utrophin. We next investigated luminal polarization by observing P-gp (Figures 4E–4H)

and multidrug resistant protein-2 (Figures 4I–4L), two important ABC proteins localized to the luminal face of vessels. The EC monoculture tubes were unable to localize either P-gp (Figure 4E) or multidrug resistant protein-2 (Figure 4I) inside the lumen as the staining appears predominantly on the outer side of the tubes or in a random distribution pattern. Astrocyte cocultures, however, showed proper localization of both proteins (Figures 4F–4J) to the luminal face as indicated by the central green staining that is

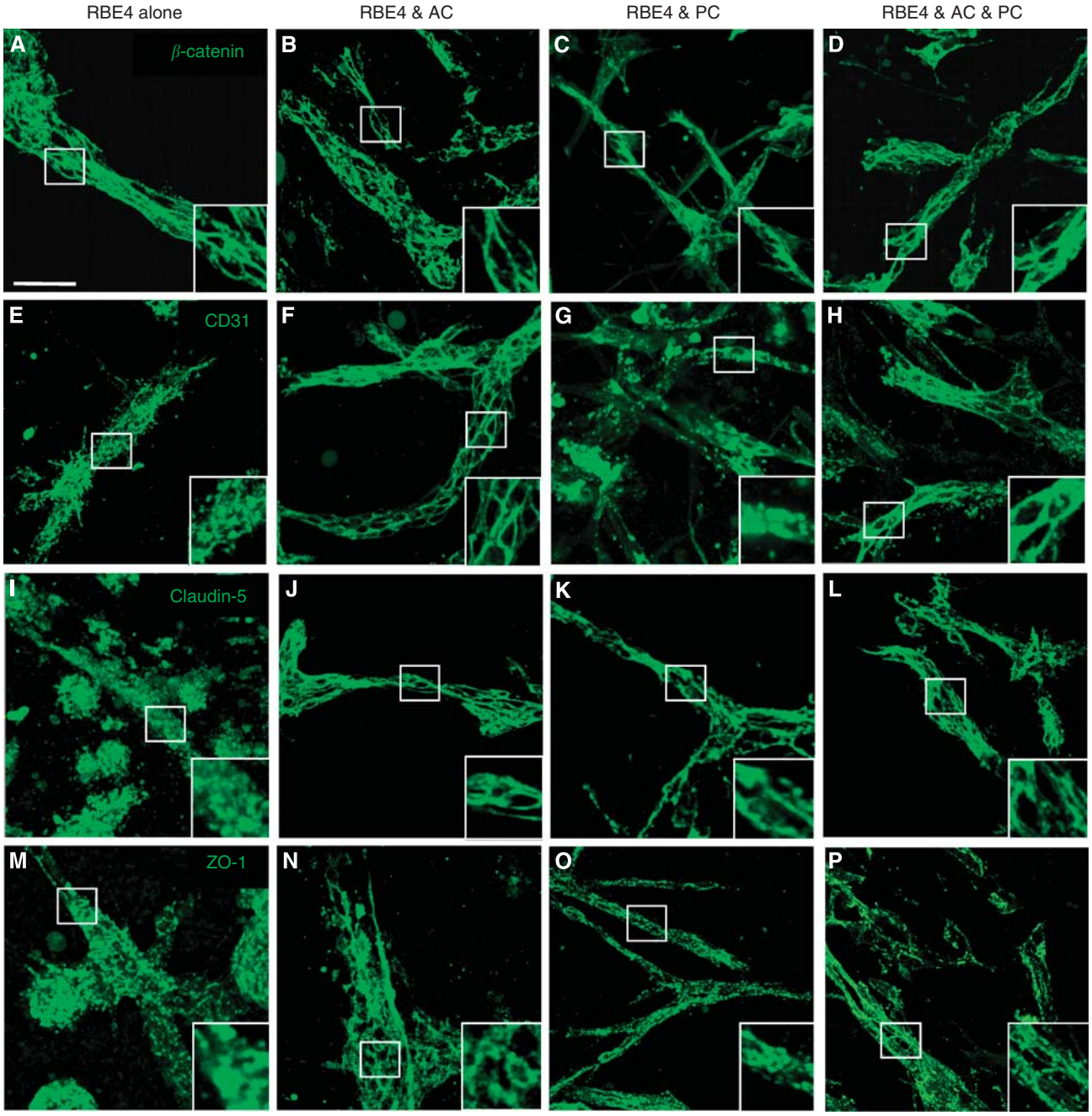

Figure 3 Astrocytes (AC) and pericytes (PC) induce barrier maturation phenotype. β-Catenin (**A**–**D**), CD31 (**E**–**H**), claudin-5 (**I**–**L**), and zonula occludens-1 (ZO-1) (**M**–**P**) immunocytochemistry fluorescent micrograph pictures obtained from RBE4 cells cultured alone or in the presence of AC and PC. Note the absence of distinct tight junctions (TJs) localization at cell–cell borders in RBE4 monocultures as seen with both claudin-5 (**I**) and ZO-1 (**M**). Inserts are magnified images of regions highlighted by boxed areas. Scale bar = 50 μm. Electron micrograph pictures from 5 day cocultures (**Q**) and RBE4 monocultures (**R**). Boxed out regions are shown as magnified pictures on the right-hand side. In the coculture image (**Q**), note the presence of electron-dense particles at the cell border (arrowheads), illustrating the presence of a TJ structure. Scale bar = 500 nm. In contrast, note the absence of such particles at cell–cell borders in monocultures (**R**), indicating the absence of TJ structures in endothelial cells cultured alone. Scale bar = 2 μm. Endo, endothelial cells; Coll, collagen matrix; Ap, astrocyte/pericyte.

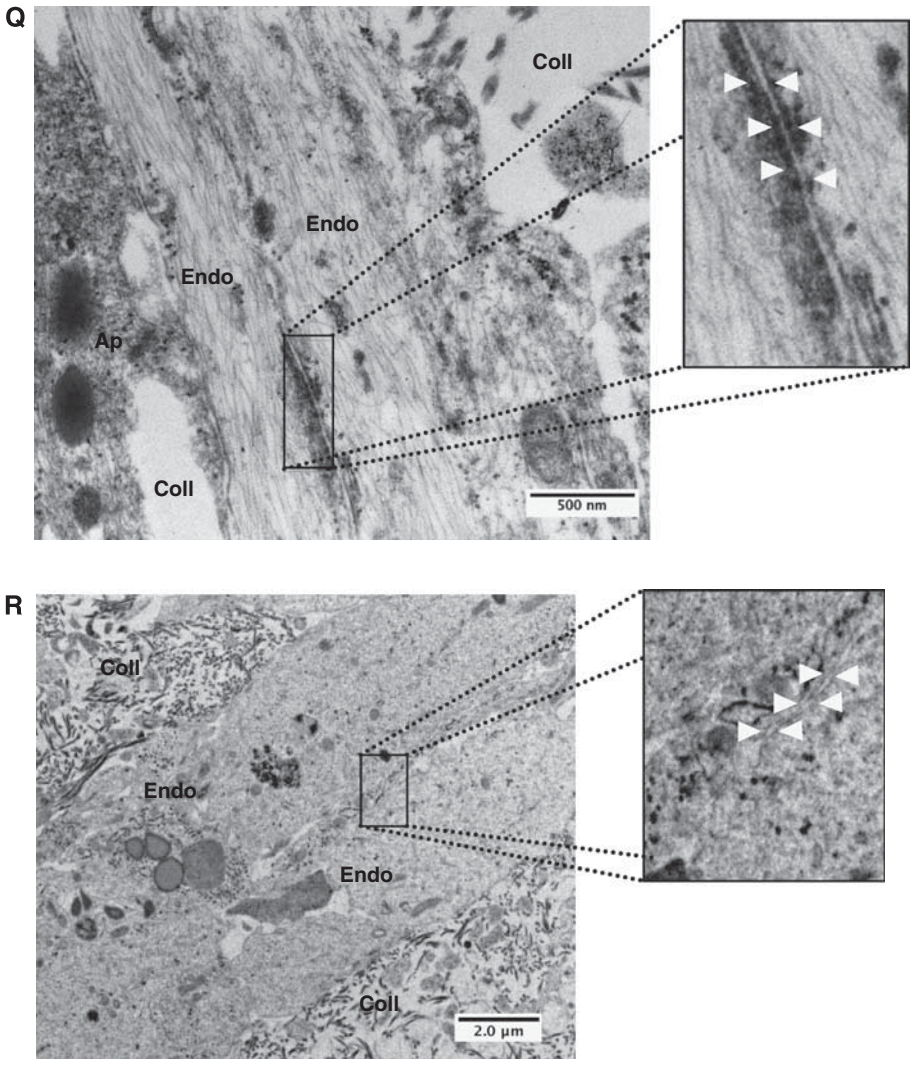

Figure 3 Continued.

facing the lumen, and red peripheral EC-specific marker. Similar observations were obtained for pericyte (Figures 4G–4K) and three-cell cocultures (Figures 4H–4L). Thus, luminal tube polarization requires the presence of astrocytes and pericytes.

Functional Validity: P-Glycoprotein Activity of the Three-Dimensional Model

Although astrocytes and pericytes induced many characteristic features of a proper BBB phenotype, the integrity and functionality of the vessels within the model remained unclear. To simultaneously address these points, activity of the P-gp transporter was examined RBE4 monocultures as well as astrocyte and three-cell cocultures using an NBD-CsA assay (Figures 4M–4Q), a functional method used to assess P-gp activity in isolated brain microvessels (Miller *et al*, 2000). Notably, P-gp activity was undetectable in RBE4 monocultures (data not shown), suggesting that functional transporter activity does not occur in tube-like structures formed solely by endothelial cells. In complete contrast, the tubes of cocultures showed high affinity for NBD-CsA (Figures 4M–4R), as observed by homogenous localization to all structures. Cross-sections of astrocyte cocultures generated by image reconstruction (Figure 4M') showed that NBD-CsA accumulates in the luminal compartment of the tubes. Such observation was also present in the three-cell cocultures (Figures 4P and 4P'), suggesting efficient efflux of NBD-CsA toward the lumen by active transport. In agreement, inhibition of such active transport by addition of either KCN (Figures 4N and 4Q) or verapamil (Figures 4O and 4R), potent inhibitors of P-gp activity, completely abrogated luminal accumulation of NBD-CsA. Cross-sectional views (Figures 4N', 4Q', 4O', and 4R') clearly show the dye still localizes to the tubes but is absent from the luminal space (asterisk). These data provide strong evidence that the ABC transporters located at the luminal side of the tubes are functionally active. Furthermore, luminal accumulation of the dye suggests vascular integrity.

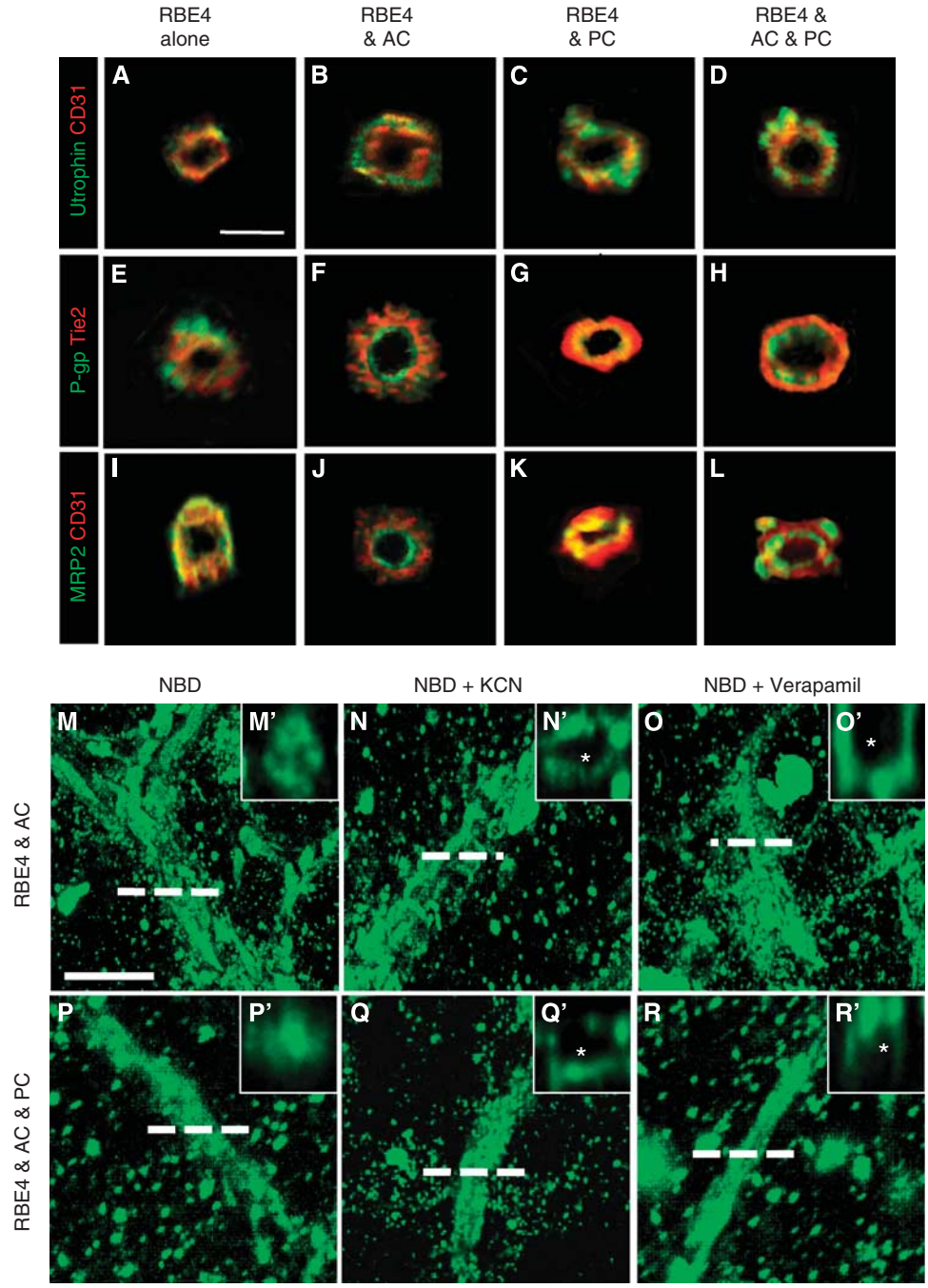

Figure 4 Astrocytes and pericytes induce tube polarity and P-glycoprotein (P-gp) activity. (**A**–**L**) Immunocytochemistry double staining and subsequent *z*-stack image reconstruction was used to obtain cross-sections of tube-like structures formed in astrocyte and pericyte cocultures. CD31 and Tie-2, endothelial markers that are not polarized, enable us to view the endothelial cells. Utrophin localization (**A**–**D**) occurred on the basolateral side of the tubes in all groups, whereas the presence of astrocytes and pericytes were required to induce proper luminal polarity, as observed with P-gp (**E**–**H**) and multidrug resistant protein-2 (MRP2) (**I**–**L**) staining. Scale bar = 10 μm. (**M**–**R**) Live imaging combined with *z*-stack image reconstruction was used to obtain fluorescent micrograph pictures of coculture tube cross-sections after incubation with (*N*-(4-nitrobenzofurazan-7-yl)-D-Lys^{8})-cyclosporin A (NBD-CsA), a substrate for P-gp, in absence (**M**, **P**) or the presence of the P-gp inhibitors KCN (**N**, **Q**) or verapamil (**O**, **R**). Note the absence of NBD-CsA accumulation within the lumen (indicated with an asterisk) in the presence of either KCN or verapamil in high power images (**N'**, **O'**, **Q'**, and **R'**). Scale bar = 50 μm.

Astrocytes and Pericytes Differentially Regulate the Vascular Responses to Hypoxic Insult

To observe whether our model is dynamic and responsive to external stimuli, and how astrocytes and pericytes modulate vascular characteristics during injury, we exposed our cultures to prolonged O_2 deprivation (48 hours at 1% O_2). Unsurprisingly, EC monocultures exhibited significantly disrupted TJ protein expression (claudin-5 and ZO-1, Figure 5E)

at EC borders of vascular structures. Both astrocytes (Figures 5B and 5F) and pericytes (Figures 5C and 5G) significantly improved tube morphology and localization of TJ proteins, although some disruption was still evident. Notably, astrocytes seemed to maintain localization of claudin-5 better than pericyte cocultures. Coculture with both cells was a prerequisite for optimal localization of both claudin-5 and ZO-1 staining to cell borders and good preservation of tube morphology (Figures 5D and 5H).

Next, we investigated how O_2 deprivation stress compromises astrocyte and pericyte interactions. We firstly monitored changes in tube diameter during hypoxic exposure in our different culturing conditions

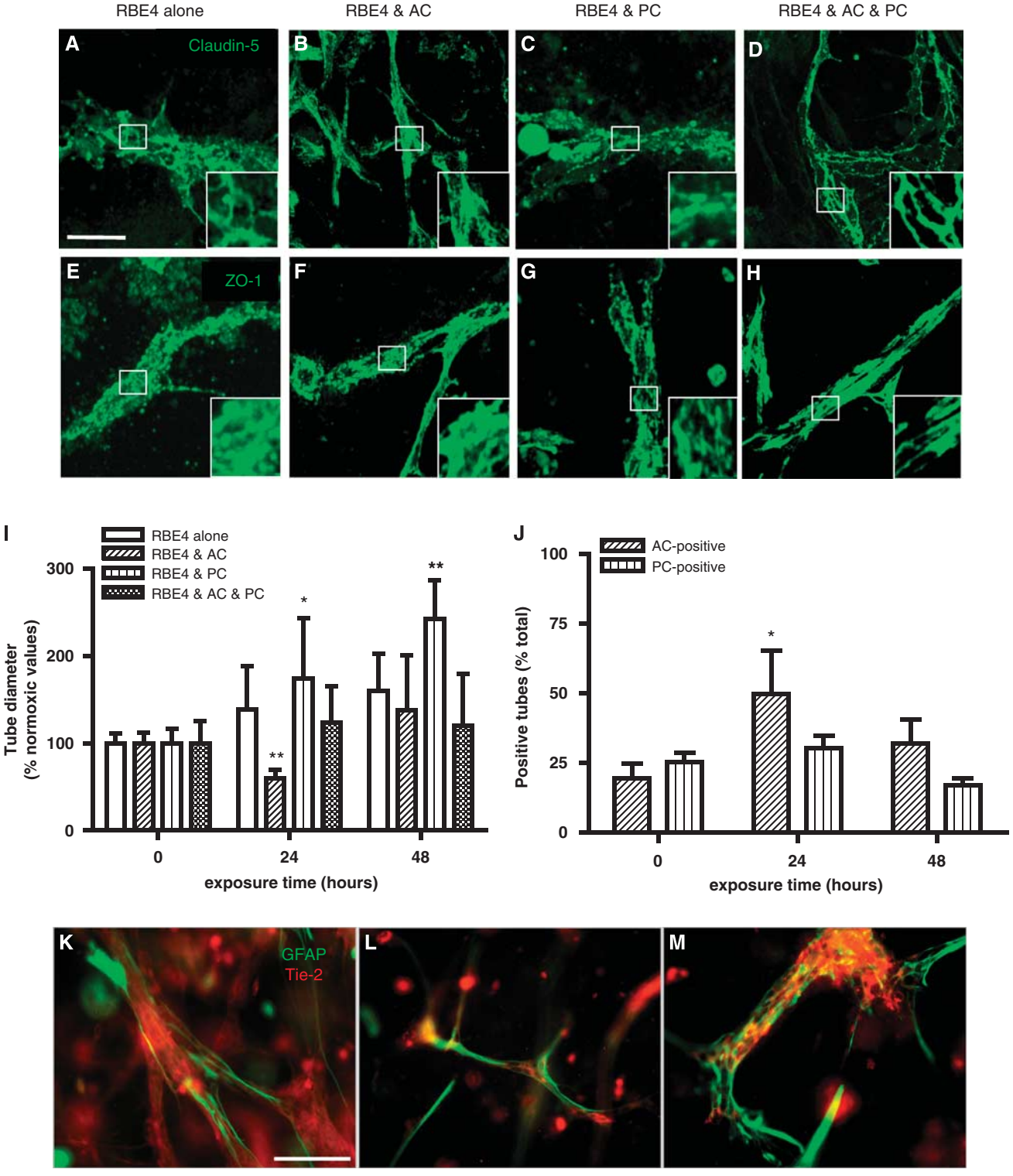

(Figure 5I). In RBE4 monocultures, tube diameter showed a modest increase reaching a maximal value of 159.93% ± 42.65% after 48 hours of exposure. Interestingly, astrocyte cocultures displayed a biphasic response, with a significant diameter decrease at 24 hours (59.76% ± 9.93%) followed by a reestablishment to values slightly over the baseline (137.55% ± 62.89%). Pericytes induced significantly high and sustained increases, with values of 174.85% ± 68.24% and 242.55% ± 43.87% at 24 and 48 hours of hypoxia, respectively. In three-cell cocultures, astrocyte responses again seemed to dominate as only small increases were observed at 24 and 48 hours (123.87% ± 42.23% and 120.37% ± 59.19%, respectively). Next, we investigated whether hypoxic stress acts as a positive or negative stimulus for astrocyte and pericyte recruitment to the tubes in three-cell cocultures (Figure 5J). Under normoxia, the number of tubes contacted by astrocytes or pericytes appeared modest (19.64% ± 5.31% and 25.33% ± 7.18%, respectively). Surprisingly, during hypoxia, the number of tubes contacted by astrocytes rapidly increased at 24 hours (49.76% ± 15.69%) before decreasing again at 48 hours (32.01% ± 8.53%). Notably, pericyte contact was not significantly altered showing values of 30.84% ± 10.02% and 17.06% ± 4.75% at 24 and 48 hours, respectively. These results clearly suggest that hypoxia differentially affects astrocyte–endothelial and pericyte–endothelial interactions.

We additionally used immunocytochemistry to monitor the changes in astrocyte–endothelial interactions by observing the density of coverage of EC tubes in astrocyte cocultures (Figures 5K–5M). Under normoxic conditions (Figure 5K), the astrocyte processes contacted EC tube-like structures. As observed previously, hypoxic exposure (24 hours at 1% O_2; Figure 5J) decreased tube diameters and surprisingly increased process coverage. Extended hypoxic exposure (48 hours at 1% O_2; Figure 5M) significantly increased tube diameter, disrupted astrocyte process morphology, and reduced tube coverage. Thus, oxygen deprivation constitutes an important modulator of TJ proteins and cellular contacts.

Discussion

Coordinated complex signaling mechanisms and pathways that exist between ECs, astrocytes, and pericytes are important for ontogeny and maintenance of the BBB *in vivo*. We are convinced that spatial cellular organization also regulates important signaling networks crucial for proper BBB function, and represents a critical missing part of our understanding. Therefore, a major goal of this study was to design and establish a novel 3D *in vitro* model system that closely mimics barrier formation *in vivo*. Such a model can be used to study both developmental and maturational aspects of BBB function, and importantly the contribution of individual cell types, namely astrocytes and pericytes, to these processes.

Our culture displayed classic EC morphogenesis such as formation of cysts, intercystal connections, and tube-like structures that appear analogous to those observed during vascular development in vertebrates such as blood islands, primary vascular plexus, and angiogenic blood vessels (Baldessari and Mione, 2008). These features reflect an innate ability of ECs, but the absence of proper ABC transporter and junctional protein localization in tube-like structures indicates an important limitation of the monocultures. Notably, astrocyte and pericyte interactions were required to induce adequate AJ and TJ complex localization and EC tube polarization in 3D, an observation correlating well with establishment of improved barrier phenotype in 2D *in vitro* coculture models (Al Ahmad *et al*, 2009; Nakagawa *et al*, 2009). Thus, our data support the concept that 3D culturing is important not only for cell structure and organization but also that both astrocytes and pericytes have defined roles in inducing barrier characteristics. Furthermore, during development of this model, the time-dependent expression and secretion of well-described mediators of angiogenesis correlates well with both ongoing morphogenesis of the system and data from previous *in vitro* and *in vivo* studies (Fredriksson *et al*, 2004; Ramsauer and D'Amore, 2007). Thus, this model represents an *in vitro* system that reflects many aspects of barrier development *in vivo*. Importantly, our data underline the fact that more frequent combined use of astrocytes and pericytes in currently existing *in vitro* models may provide additional information on BBB characteristics.

Our model also provides fundamental information on the modulation of tubulogenesis by astrocytes and pericytes. Pericytes increased the number of tubes thereby mediating a pro-angiogenic phenotype on ECs agreeing with previous studies (Murata *et al*, 1994; Watanabe *et al*, 1997). The presence of astrocytes on the other hand seemed to alter

Figure 5 Astrocytes (AC) and pericytes (PC) differentially modulate RBE4 tube responses to hypoxic stimulus. (**A**–**H**) The presence of both AC and PC is required to maintain tight junctions (TJs) complex localization at cell–cell borders in cultures exposed to prolonged hypoxia (1% O_2 for 48 hours). Note that astrocyte cocultures (AC) appear to support better maintenance than pericyte cocultures (PC), as seen in high power inserts. Scale bar = 50 μm. (**I**) The AC and PC modulate tube diameter in hypoxic cultures. Diameters are expressed as the percentage of their respective normoxic values. Note the transient decrease in diameter observed in AC cocultures, whereas PC cocultures induce a continuous increase in diameter over time. The pericyte effect is blunted in the three-cell cocultures. $n = 20$; $^*P < 0.05$ and $^{**}P < 0.01$ against normoxic values. (**J**) Hypoxia transiently increases AC coverage of endothelial tubes, whereas no significant alteration in PC coverage was observed. $^*P < 0.05$ compared with normoxic values, $n = 5$. (**K**–**M**) Hypoxia acts as a biphasic stimulus for astrocyte–endothelial interactions. Immunocytochemistry confirms increased glial fibrillary acidic protein (GFAP +) staining (green) over the RBE4 tubes (red) after 24 hours (**L**) compared with normoxia (**K**). Prolonged exposure (48 hours) decreases GFAP + staining over the tubes and induces an increase in tube diameter. Scale bar = 50 μm.

vasculogenic and angiogenic-like processes in favor of vessel maturation. Intriguing differential effects were also observed on tube diameters. Interestingly, consistent abolishment of the pericyte pro-angiogenic stimulus in the presence of astrocytes suggests that astrocytes may compete with or suppress the action of pericytes. *In vivo* pericytes are the first cells to interact with cerebral microvessels during early embryogenesis (Virgintino *et al*, 2007), whereas astrocyte–EC interactions are initiated only in the late developmental stages when maturation of the BBB occurs (Butt *et al*, 1990; Ogunshola *et al*, 2000). We can therefore speculate that pericytes promote tube formation during early development to provide the developing central nervous system with optimal O_2 and nutrient supply. Once neurogenesis declines and neuronal differentiation is initiated, newly differentiated astrocytes might inhibit the pericytic pro-angiogenic effect and induce BBB maturation. Notably, we recently highlighted the existence of such cellular cross-talk between these two cells during physiological conditions as well as O_2 deprivation stress (Al Ahmad *et al*, 2009; Schmid-Brunclik *et al*, 2008).

Contact of both astrocytes and pericytes with the vascular structures improved barrier protein localization, although astrocytes seemed to perform better than pericytes. Despite this, both cells effectively induced luminal efflux and accumulation of a P-gp substrate demonstrating not only the presence and activation of an efficient transport mechanism but also vascular integrity (Bauer *et al*, 2004; Miller *et al*, 2000; Soontornmalai *et al*, 2006). This and our previous study highlight that pericytes alone can maintain barrier characteristics and thus enable vascular structures devoid of astrocytes to function efficiency.

Hypoxia, a characteristic state that disrupts the BBB in many pathologies (Brown and Davis, 2005; Hopfl *et al*, 2003), modulates both protein localization and cellular interactions within the model system. Surprisingly, acute hypoxia initially increased astrocyte coverage of tube structures, whereas prolonged hypoxia triggered loss of astrocyte contacts and vascular swelling as occurs during injury *in vivo* (Yang *et al*, 2007). In complete contrast, pericyte coverage remained unaltered. We speculate that these acute responses represent short-term measures to maintain BBB function during injurious stimuli that are lost during prolonged injury. These observations correlate with the fact that TJ protein localization during acute insult, as well as vascular integrity (Al Ahmad *et al*, 2009), is better maintained by astrocytes, whereas pericytes are more effective during prolonged injury. Understanding the cross-talk that exists between astrocytes and pericytes to modulate such pathways could possibly be exploited in future to regulate both vascular development and integrity of the BBB. Determinations of such signaling pathways are now being investigated using this model system.

In conclusion, our results emphasize an important role of pericytes, in addition to astrocytes, in BBB development and maintenance. It is clear that pericytes contribute significantly to vasculogenic/angiogenic processes and have functions distinct from astrocytes that define BBB characteristics. Overall, our model represents an exciting tool to investigate different aspects of BBB function that include, but are not limited to developmental processes, temporal-spatial effects of different cell types (such as neurons, inflammatory cells, etc.) and the impact of various external factors and stimuli on cellular interactions. We are confident that this innovative tool will provide a new dimension to our understanding of the cellular interactions at the BBB during physiological and pathological states, and bring us significantly forward in many fields of research.

Acknowledgements

The authors thank Dr B Bauer for the NBD-CsA, Dr JM Fritschy for the ABC transporter antibodies, G Barmettler (Zurich Microscopy Center, ZMB) for the preparation of transmitted electron microscopy samples, Drs A Hehl (Institute of Parasitology, University of Zurich) and U Ziegler (ZMB) for providing access to both confocal microscope and Imaris software, and Dr J Badaut for fruitful discussions.

Disclosure/conflict of interest

The authors declare no conflict of interest.

References

Al Ahmad A, Gassmann M, Ogunshola OO (2009) Maintaining blood-brain barrier integrity: pericytes perform better than astrocytes during prolonged oxygen deprivation. *J Cell Physiol* 218:612–22

Baldessari D, Mione M (2008) How to create the vascular tree? (Latest) help from the zebrafish. *Pharmacol Ther* 118:206–30

Banks WA, Ercal N, Price TO (2006) The blood-brain barrier in neuroAIDS. *Curr HIV Res* 4:259–66

Bauer B, Hartz AM, Fricker G, Miller DS (2004) Pregnane X receptor up-regulation of P-glycoprotein expression and transport function at the blood-brain barrier. *Mol Pharmacol* 66:413–9

Bell E, Ivarsson B, Merrill C (1979) Production of a tissue-like structure by contraction of collagen lattices by human fibroblasts of different proliferative potential *in vitro*. *Proc Natl Acad Sci USA* 76:1274–8

Brightman MW, Reese TS (1969) Junctions between intimately apposed cell membranes in the vertebrate brain. *J Cell Biol* 40:648–77

Brown RC, Davis TP (2005) Hypoxia/aglycemia alters expression of occludin and actin in brain endothelial cells. *Biochem Biophys Res Commun* 327:1114–23

Butt AM, Jones HC, Abbott NJ (1990) Electrical resistance across the blood-brain barrier in anaesthetized rats: a developmental study. *J Physiol* 429:47–62

Chow J, Ogunshola O, Fan SY, Li Y, Ment LR, Madri JA (2001) Astrocyte-derived VEGF mediates survival and tube stabilization of hypoxic brain microvascular endothelial cells *in vitro*. *Brain Res Dev Brain Res* 130:123–32

Dehouck MP, Meresse S, Delorme P, Fruchart JC, Cecchelli R (1990) An easier, reproducible, and mass-production method to study the blood-brain barrier *in vitro*. *J Neurochem* 54:1798–801

del Zoppo GJ, Mabuchi T (2003) Cerebral microvessel responses to focal ischemia. *J Cereb Blood Flow Metab* 23:879–94

Dore-Duffy P (2003) Isolation and characterization of cerebral microvascular pericytes. *Methods Mol Med* 89:375–82

Engelhardt B (2008) The blood-central nervous system barriers actively control immune cell entry into the central nervous system. *Curr Pharm Des* 14:1555–65

Fredriksson L, Li H, Eriksson U (2004) The PDGF family: four gene products form five dimeric isoforms. *Cytokine Growth Factor Rev* 15:197–204

Hawkins BT, Davis TP (2005) The blood-brain barrier/neurovascular unit in health and disease. *Pharmacol Rev* 57:173–85

Hopfl G, Ogunshola O, Gassmann M (2003) Hypoxia and high altitude. The molecular response. *Adv Exp Med Biol* 543:89–115

Janzer RC, Raff MC (1987) Astrocytes induce blood-brain barrier properties in endothelial cells. *Nature* 325: 253–7

Kaur C, Ling EA (2008) Blood brain barrier in hypoxic-ischemic conditions. *Curr Neurovasc Res* 5:71–81

Koh W, Stratman AN, Sacharidou A, Davis GE (2008) *In vitro* three dimensional collagen matrix models of endothelial lumen formation during vasculogenesis and angiogenesis. *Methods Enzymol* 443:83–101

Kulik T, Kusano Y, Aronhime S, Sandler AL, Winn HR (2008) Regulation of cerebral vasculature in normal and ischemic brain. *Neuropharmacology* 55:281–8

Lee SR, Wang X, Tsuji K, Lo EH (2004) Extracellular proteolytic pathophysiology in the neurovascular unit after stroke. *Neurol Res* 26:854–61

Ment LR, Stewart WB, Scaramuzzino D, Madri JA (1997) An *in vitro* three-dimensional coculture model of cerebral microvascular angiogenesis and differentiation. *In Vitro Cell Dev Biol Anim* 33:684–91

Miller DS, Nobmann SN, Gutmann H, Toeroek M, Drewe J, Fricker G (2000) Xenobiotic transport across isolated brain microvessels studied by confocal microscopy. *Mol Pharmacol* 58:1357–67

Murata T, Ishibashi T, Inomata H, Sueishi K (1994) Media conditioned by coculture of pericytes and endothelial cells under a hypoxic state stimulate *in vitro* angiogenesis. *Ophthalmic Res* 26:23–31

Nakagawa S, Deli MA, Kawaguchi H, Shimizudani T, Shimono T, Kittel A, Tanaka K, Niwa M (2009) A new blood-brain barrier model using primary rat brain endothelial cells, pericytes and astrocytes. *Neurochem Int* 54:253–63

Neuwelt E, Abbott NJ, Abrey L, Banks WA, Blakley B, Davis T, Engelhardt B, Grammas P, Nedergaard M, Nutt J, Pardridge W, Rosenberg GA, Smith Q, Drewes LR (2008) Strategies to advance translational research into brain barriers. *Lancet Neurol* 7:84–96

Ogunshola OO, Stewart WB, Mihalcik V, Solli T, Madri JA, Ment LR (2000) Neuronal VEGF expression correlates with angiogenesis in postnatal developing rat brain. *Brain Res Dev Brain Res* 119:139–53

Pardridge WM (1999) Blood-brain barrier biology and methodology. *J Neurovirol* 5:556–69

Ramsauer M, D'Amore PA (2007) Contextual role for angiopoietins and TGFbeta1 in blood vessel stabilization. *J Cell Sci* 120:1810–7

Roux F, Durieu-Trautmann O, Chaverot N, Claire M, Mailly P, Bourre JM, Strosberg AD, Couraud PO (1994) Regulation of gamma-glutamyl transpeptidase and alkaline phosphatase activities in immortalized rat brain microvessel endothelial cells. *J Cell Physiol* 159:101–13

Schmid-Brunclik N, Burgi-Taboada C, Antoniou X, Gassmann M, Ogunshola OO (2008) Astrocyte responses to injury: VEGF simultaneously modulates cell death and proliferation. *Am J Physiol Regul Integr Comp Physiol* 295:R864–73

Soontornmalai A, Vlaming ML, Fritschy JM (2006) Differential, strain-specific cellular and subcellular distribution of multidrug transporters in murine choroid plexus and blood-brain barrier. *Neuroscience* 138:159–69

Virgintino D, Girolamo F, Errede M, Capobianco C, Robertson D, Stallcup WB, Perris R, Roncali L (2007) An intimate interplay between precocious, migrating pericytes and endothelial cells governs human fetal brain angiogenesis. *Angiogenesis* 10:35–45

Warren MS, Zerangue N, Woodford K, Roberts LM, Tate EH, Feng B, Li C, Feuerstein TJ, Gibbs J, Smith B, de Morais SM, Dower WJ, Koller KJ (2009) Comparative gene expression profiles of ABC transporters in brain microvessel endothelial cells and brain in five species including human. *Pharmacol Res* 59:404–13

Watanabe S, Morisaki N, Tezuka M, Fukuda K, Ueda S, Koyama N, Yokote K, Kanzaki T, Yoshida S, Saito Y (1997) Cultured retinal pericytes stimulate *in vitro* angiogenesis of endothelial cells through secretion of a fibroblast growth factor-like molecule. *Atherosclerosis* 130:101–7

Yang Y, Estrada EY, Thompson JF, Liu W, Rosenberg GA (2007) Matrix metalloproteinase-mediated disruption of tight junction proteins in cerebral vessels is reversed by synthetic matrix metalloproteinase inhibitor in focal ischemia in rat. *J Cereb Blood Flow Metab* 27:697–709

Zerlin M, Goldman JE (1997) Interactions between glial progenitors and blood vessels during early postnatal corticogenesis: blood vessel contact represents an early stage of astrocyte differentiation. *J Comp Neurol* 387:537–46

Zlokovic BV (2008) The blood-brain barrier in health and chronic neurodegenerative disorders. *Neuron* 57: 178–201

Supplementary Information accompanies the paper on the Journal of Cerebral Blood Flow & Metabolism website (http://www.nature.com/jcbfm)